Spiral Dinuclear Complexes of Tetradentate N_4 Diazine Ligands with Mn(II), Fe(II), Fe(III), Co(III), and Ni(II) Salts

Zhiqiang Xu,[†] Laurence K. Thompson,*[,†] David O. Miller,[†] Howard J. Clase,[†] Judith A. K. Howard,[‡] and Andrés E. Goeta[‡]

Departments of Chemistry, Memorial University of Newfoundland, St. John's, Newfoundland A1B 3X7, Canada, and University of Durham, Durham DH1 3LE, U.K.

Received December 16, 1997

A series of dinuclear complexes of the tetradentate dipyridyl−diazine ligand PAHAP with Mn(II), Fe(II), Fe(III), Co(III), and Ni(II) salts is reported in which three ligands wrap themselves around the six-coordinate metal centers in a rare spiral-like fashion. A similar Fe(II) complex is found for the dipyrazinyl−diazine ligand PZHPZ. The ligands are severely twisted with dihedral angles between the metal chelate ring mean planes on each ligand in the range 50−70°, values close to the expected twist angle for orthogonality between the bridging nitrogen atom p orbitals. Full structures are reported for the dinuclear complexes $[Mn_2(PAHAP)_3](ClO_4)_4 \cdot 5H_2O$ (**1**), $[Fe_2(PAHAP)_3](NO_3)_4 \cdot 3H_2O$ (**2**), $[Fe_2(PZHPZ)_3](NO_3)_4 \cdot 5H_2O$ (**5**), $[Co_2(PAHAP)_3](NO_3)_6 \cdot 5H_2O$ (**6**), and $[Ni_2(PAHAP)_3][Ni(H_2O)_6](NO_3)_6 \cdot 4.5H_2O$ (**7**). Other derivatives $[Fe_2(PAHAP)_3](ClO_4)_4 \cdot 4H_2O$ (**3**), $[Fe_2(PAHAP)_3](ClO_4)_6 \cdot 4.5H_2O$ (**4**), $[Ni_2(PAHAP)_3](ClO_4)_4 \cdot 5H_2O$ (**8**), and $[Fe(PHAAP\text{-}H)(H_2O)_2(NO_3)](NO_3)_2$ (**9**) are also reported. Complex **1** crystallized in the monoclinic system, space group $C2/c$, with $a = 13.4086(2)$ Å, $b = 32.0249(1)$ Å, $c = 14.3132(2)$ Å, $\alpha = 90°$, $\beta = 115.635(1)°$, $\gamma = 90°$, and $Z = 4$. Complex **2** crystallized in the cubic system, space group $Pa\bar{3}$, with $a = b = c = 21.0024(1)$ Å, $\alpha = \beta = \gamma = 90°$, and $Z = 8$. Complex **5** crystallized in the monoclinic system, space group $P2/n$, with $a = 14.039(3)$ Å, $b = 11.335(6)$ Å, $c = 14.6517(15)$ Å, $\beta = 96.852(11)°$, and $Z = 1$. Complex **6** crystallized in the trigonal system, space group $R\bar{3}c(h)$, with $a = b = 17.386(2)$ Å, $c = 32.15(2)$ Å, $\alpha = \beta = 90°$, $\gamma = 120°$, and $Z = 4$. Complex **7** crystallized in the trigonal system, space group $R\bar{3}c$, with $a = b = 17.3737(3)$ Å, $c = 33.235(6)$ Å, $\alpha = \beta = 90°$, $\gamma = 120°$, and $Z = 27$. Weak ferromagnetic coupling was observed for **1** ($2J = 2.1$ cm^{-1}), and no coupling was observed for the dinuclear Ni(II) centers in **7** and **8**. **2**, **3**, and **5** are low-spin Fe(II) systems.

Introduction

Diazine ligands based on a single N−N bond as the dinucleating focus have received moderate attention over the years, beginning with the early work of Busch on pyridine aldazine (PAA; Figure 1).[1,2] The dinuclear complexes described were shown to contain the cation $[M_2(PAA)_3)]^{4+}$ (M = Fe(II), Co(II), Ni(II)), but no structures were reported. Magnetic moments indicated that the Fe(II) centers were low spin and the cobalt(II) centers high spin. A subsequent variable-temperature magnetic study by Blake[3] showed that the dinuclear cation $[Ni_2(PAA)_3]^{4+}$ contained weakly coupled nickel(II) centers ($-J/k = 8.3-13.7°$), supporting the dinuclear nature and proposed spiral structure of this class of complex, and the presence of intramolecular exchange coupling. Similar complexes of the related ligand 2-pyridyl methyl ketazine (PMK; Figure 1) $\{[M_2(PMK)_3]^{4+}$ (M = Fe(II), Co(II), Ni(II))$\}$ were reported in 1970[4] with similar magnetic properties.

The first structure of this type was reported in 1974 for the complex $[Co_2(PMK)_3]ZnCl_4 \cdot [ZnCl_3(H_2O)]_2 \cdot 4H_2O$,[5] which was shown to have the expected spiral-like arrangement of three tetradentate ligands around the two distorted octahedral Co(II) centers, with the diazine nitrogens forming the triple bridge. The Co−Co distance is 3.81(1) Å, and the average Co−N−N−Co dihedral angle 44°, indicating a significant twist of the three ligands about the Co−Co vector. Another report[6] documents the structure of the complex $[Cu_2(PMK)Cl_4]$ (Figure 1), which involves two four-coordinate Cu(II) centers bridged again

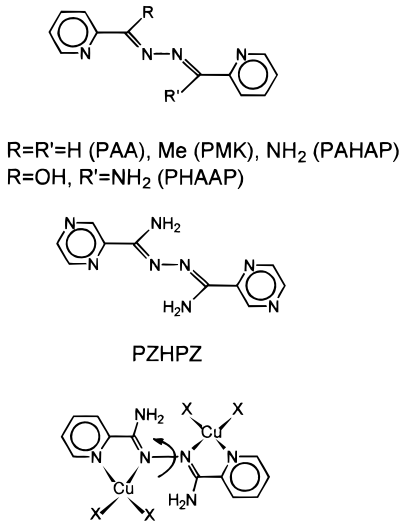

Figure 1. Diazine ligands and the dicopper model.

* Corresponding author. Fax: 709-737-3702. E-mail: lthomp@morgan.ucs.mun.ca.
[†] Memorial University of Newfoundland.
[‡] University of Durham.

(1) Stratton, W. J.; Busch, D. H. *J. Am. Chem. Soc.* **1958**, *80*, 1286.
(2) Stratton, W. J.; Busch, D. H. *J. Am. Chem. Soc.* **1960**, *82*, 4834.
(3) Ball, P. W.; Blake, A. B. *J. Chem. Soc. A* **1969**, 1415.
(4) Stratton, W. J. *Inorg. Chem.* **1970**, *9*, 317.
(5) Boyd, P. D. W.; Gerloch, M.; Sheldrick, G. M. *J. Chem. Soc., Dalton Trans.* **1974**, 1097.

S0020-1669(97)01576-0 CCC: $15.00
Published on Web 06/25/1998

by the diazine group, in a twisted arrangement, with a Cu−N−N−Cu dihedral angle of 70.8°. This complex exhibits weak antiferromagnetic coupling ($-2J = 52$ cm^{-1}). A more recent report describes the neutral Fe(III) complex $[Fe_2(salhn)_3]\cdot CH_3CN$ (salhn = *N*,*N*′-bis(salicylidene)hydrazine), which contains a spiral, dinuclear center with an unsymmetrical arrangement of two Fe(III) ions bridged by three N−N bridges and exhibits weak antiferromagnetic coupling.[7]

A related dipyridyl diazine is PAHAP (picolinamide azine; Figure 1), which contains additional donor (NH_2) groups, has several potential modes of bonding which could produce both mononuclear and dinuclear complexes, and also has the ability to act as a hexadentate ligand. The related, potentially octadentate ligand PZHPZ (Figure 1) has additional donor capacity in the external pyrazine nitrogen donor sites. A series of dinuclear copper(II) complexes of PAHAP has already been reported (Figure 1) and displays the unique feature of intramolecular exchange coupling which is dependent upon the degree of molecular twist of the magnetic planes about the N−N bond, with ferromagnetic exchange at small angles (<80°) and antiferromagnetic exchange at larger angles.[8,9] In this report, the spiral dinuclear complexes $[Mn_2(PAHAP)_3](ClO_4)_4\cdot 5H_2O$ (**1**), $[Fe_2(PAHAP)_3](NO_3)_4\cdot 3H_2O$ (**2**), $[Fe_2(PAHAP)_3](ClO_4)_4\cdot 4H_2O$ (**3**), $[Fe_2(PAHAP)_3](ClO_4)_6\cdot 4.5H_2O$ (**4**), $[Fe_2(PZHPZ)_3](NO_3)_4\cdot 5H_2O$ (**5**), $[Co_2(PAHAP)_3](NO_3)_6\cdot 3H_2O$ (**6**), $[Ni_2(PAHAP)_3][Ni(H_2O)_6](NO_3)_6\cdot 4.5H_2O$ (**7**), and $[Ni_2(PAHAP)_3](ClO_4)_4\cdot 5H_2O$ (**8**) and the mononuclear complex $[Fe(PHAAP\text{-}H)(H_2O)_2(NO_3)](NO_3)_2$ (**9**) are described. Structures are reported for **1**, **2**, **5**−**7**, and **9**. The same twisted, spiral-like dinuclear cation exists in all these structures, with the diazine nitrogen pairs bridging the two metal centers and the NH_2 groups remaining uncoordinated on the exterior of the dinuclear cationic fragment. Room-temperature and variable-temperature magnetic properties are discussed in relation to structure and those of the related complexes of PAA and PMK. The unusual mononuclear complex **9** results from the reaction of $Fe(NO_3)_3\cdot 9H_2O$ and PAHAP in water, which also produces **2**. **9** contains the ligand PHAAP (Figure 1), formed by decomposition of PAHAP.

Experimental Section

Physical Measurements. Infrared spectra were recorded as Nujol mulls using a Mattson Polaris FT-IR instrument. UV/vis spectra were recorded in the solid state (mull transmittance) and solution using a Cary 5E spectrometer. Mass spectra were obtained using a VG Micromass 7070HS spectrometer. Microanalyses were carried out by the Canadian Microanalytical Service, Delta, Canada. Room-temperature magnetic susceptibilities were measured by the Faraday method using a Cahn 7600 Faraday magnetic balance, and variable-temperature magnetic data (4−305 K) were obtained using an Oxford Instruments superconducting Faraday susceptometer with a Sartorius 4432 microbalance. A main solenoid field of 1.5 T and a gradient field of 10 T m^{-1} were employed. $HgCo(NCS)_4$ was used as a calibration standard, and temperature errors were checked with the Curie−Weiss paramagnet $[TMENH_2][CuCl_4]$ (TMEN = $(CH_3)_2N(CH_2)_2N(CH_3)_2$).[10]

Electrochemical experiments were performed at room temperature in water (distilled) under O_2-free conditions using a BAS CV27 voltammograph. A three-electrode system was employed, consisting of a glassy carbon working electrode, a platinum counter electrode, and a standard calomel (SCE) reference electrode. The supporting electrolyte was $NaNO_3$ or NEt_4NO_3 (0.1 M) with 10^{-3}−10^{-4} M solutions of complex.

Synthesis of Ligands and Complexes. PAHAP was synthesized according to a published procedure.[8] PZHPZ was synthesized in a similar fashion using 2-cyanopyrazine instead of 2-cyanopyridine. PHAAP was synthesized by the reaction of picolinic hydrazide and the methyl ester of imidopicolinic acid.[11] In some cases, lattice solvent content differs between the X-ray sample and the analytical sample, due to vacuum-drying of the sample prior to elemental analysis.

$[Mn_2(PAHAP)_3](ClO_4)_4\cdot 5H_2O$ (1), $[Fe_2(PAHAP)_3](ClO_4)_4\cdot 4H_2O$ (3), and $[Ni_2(PAHAP)_3](ClO_4)_4\cdot 5H_2O$ (8). PAHAP (0.36 g, 1.5 mmol) was added to a hot aqueous methanol (80/20) solution (40 mL) of $M(ClO_4)_2\cdot xH_2O$ (M = Mn^{2+}, Fe^{2+}, Ni^{2+}), and the mixture was stirred at room temperature for several minutes, until the ligand dissolved. The clear solution was filtered, and the filtrate was allowed to stand at room temperature overnight. Well-formed crystals were produced in each case, which were filtered off, washed quickly with cold water, and dried in air (yields 80−85%). Anal. Calcd for $[Mn_2(C_{12}H_{12}N_6)_3](ClO_4)_4\cdot 5H_2O$ (yellow) (**1**): C, 33.25; H, 3.40; N, 19.38. Found: C, 33.21; H, 2.97; N, 19.26. Calcd for $[Fe_2(C_{12}H_{12}N_6)_3](ClO_4)_4\cdot 4H_2O$ (dark red-brown) (**3**): C, 28.63; H, 3.00; N, 16.69. Found: C, 28.63; H, 3.27; N, 16.71. Calcd for $[Ni_2(C_{12}H_{12}N_6)_3](ClO_4)_4\cdot 5H_2O$ (orange brown) (**8**): C, 32.61; H, 3.50; N, 19.01. Found: C, 32.63; H, 3.31; N, 19.07.

$[Fe_2(PAHAP)_3](NO_3)_4\cdot 3H_2O$ (2), $[Fe_2(PZHPZ)_3](NO_3)_4\cdot 5H_2O$ (5), $[Co_2(PAHAP)_3](NO_3)_6]\cdot 3H_2O$ (6), $[Ni_2(PAHAP)_3][Ni(H_2O)_6](NO_3)_6\cdot 4.5H_2O$ (7), and $[Fe(PHAAP\text{-}H)(H_2O)_2(NO_3)](NO_3)_2$ (9). PAHAP (0.48 g, 2.0 mmol) was added to a warm aqueous solution (40 mL) of $M(NO_3)_x\cdot yH_2O$ (M = Fe, $x = 3$, $y = 9$; M = Co, Ni, $x = 2$, $y = 6$) (2.0 mmol). The mixture was stirred in air for a few minutes until a clear solution formed. The resultant mixture was filtered, and the filtrate was allowed to stand at room temperature for several days. The well-formed crystals that appeared were filtered off, washed with a small amount of cold water, and air-dried (yields: 30−40% for **2** and **6**; 80% for **7**). Close examination of the product in **2** revealed that it was a mixture, containing a small amount (≈20 mg) of dark, almost black rectangular prisms (**9**), in a bulk sample of dark brown octahedral-shaped crystals (**2**), which were separated by hand. **9** has been shown to be a mononuclear derivative of the hydrolyzed ligand PHAAP, derived from PAHAP. PHAAP was synthesized independently,[11] and **9** was prepared independently by reaction of PHAAP with $Fe(NO_3)_3\cdot 9H_2O$ in water. PHAAP (0.24 g, 1.0 mmol) was added to an aqueous solution (20 mL) of $Fe(NO_3)_3\cdot 9H_2O$ (0.40 g, 1.0 mmol) with stirring at room temperature. Methanol (5 mL) was added to aid solution of the ligand. Within a few minutes, a dark greenish-black clear solution formed, the mixture was filtered, and the filtrate was allowed to stand overnight. Black prismatic crystals of **9** formed, which were filtered off, washed with a small amount of cold water, and air-dried (yield 80%). **5** was prepared similarly to **2** by adding PZHPZ (0.36 g, 1.5 mmol) to an aqueous methanol (75/25) solution of $Fe(NO_3)_3\cdot 9H_2O$ (0.40 g, 1.0 mmol). The resulting dark solution was filtered, and the filtrate was allowed to stand at room temperature for several days. Dark brown crystals suitable for structural determination formed, which were filtered off, washed with a small quantity of cold water, and allowed to dry in air (yield 30%). No mononuclear derivative has so far been isolated from this reaction, but the low yield of **5** suggests that a similar hydrolysis reaction is occurring. Anal. Calcd for $[Fe_2(C_{12}H_{12}N_6)_3](NO_3)_4\cdot 3H_2O$ (red-brown) (**2**): C, 38.11; H, 3.73; N, 27.16. Found: C, 38.14; H, 3.61; N, 27.37. Calcd for $[Fe_2(C_{10}H_{10}N_8)_3](NO_3)_4\cdot 5H_2O$ (dark red-brown) (**5**): C, 30.63; H, 3.43; N, 33.32. Found: C, 30.90; H, 3.21; N, 33.20. Calcd for $[Co_2(C_{12}H_{12}N_6)_3](NO_3)_6\cdot 3H_2O$ (red) (**6**): C, 34.19; H, 3.35; N, 26.57. Found: C, 34.19; H, 3.40; N, 25.92. Calcd for $[Ni_2(C_{12}H_{12}N_6)_3]$ $[Ni(H_2O)_6](NO_3)_6\cdot 4.5H_2O$ (orange-brown) (**7**): C, 29.66; H, 3.94; N, 23.05. Found: C, 29.64; H, 4.02; N, 23.04. Calcd for $[Fe(C_{12}H_{11}N_5O)(H_2O)_2(NO_3)](NO_3)_2$ (black) (**9**): C, 27.76; H, 2.91; N, 21.58. Found: C, 27.96; H, 2.97; N, 21.53.

$[Fe_2(PAHAP)_3](ClO_4)_6\cdot 4.5H_2O$ (4). PAHAP (0.24 g, 1.0 mmol) was added to an aqueous solution (20 mL) of $Fe(ClO_4)_3\cdot 6H_2O$ (0.36 g,

(6) O'Connor, C. J.; Romananch, R. J.; Robertson, D. M.; Eduok, E. E.; Fronczek, F. R. *Inorg. Chem.* **1983**, *22*, 449.
(7) Saroja, J.; Manivannan, V.; Chakraborty, P.; Pal, S. *Inorg. Chem.* **1995**, *34*, 3099.
(8) Xu, Z.; Thompson, L. K.; Miller, D. O. *Inorg. Chem.* **1997**, *36*, 3985.
(9) Thompson, L. K.; Xu, Z.; Goeta, A. E.; Howard, J. A. K.; Clase, H. J.; Miller, D. O. *Inorg. Chem.*, in press.
(10) Brown, D. S.; Crawford, V. H.; Hall, J. W.; Hatfield, W. E. *J. Phys. Chem.* **1977**, *81*, 1303.
(11) Xu, Z.; Thompson, L. K. Unpublished results.

1.0 mmol) at room temperature. Dark brown crystals appeared within a few minutes (yield 70%). The product was filtered off, washed with a small amount of cold water, and dried in air. Anal. Calcd for $[Fe_2(C_{12}H_{12}N_6)_3](ClO_4)_6 \cdot 4.5H_2O$ (**4**): C, 28.63; H, 3.00; N, 16.69. Found: C, 28.63; H, 3.27; N, 16.71.

Crystallographic Data Collection and Refinement of the Structures. $[Ni_2(PAHAP)_3][Ni(H_2O)_6](NO_3)_6 \cdot 4.5H_2O$ (7). Crystals of **7** are orange-brown. A single crystal of **7** of dimensions 0.26 × 0.22 × 0.16 mm was attached to a quartz fiber and transferred to a Siemens SMART three-circle diffractometer with graphite-monochromatized Mo Kα X-radiation, and a CCD area detector was used for data collection.[12] ω scans were performed in such a way that four scan ranges of 180, 120, 180, and 120° in ω at 0, 88, 180, and 268 ϕ positions, respectively, were covered at 0.3° ω intervals. Cell parameters were refined using the centroid values of 462 reflections with θ angles in the range 13.7−22.6°. Raw frame data were integrated using the SAINT program[13] to $2\theta_{max} = 50.03°$. The structure was solved by direct methods and refined by full-matrix least-squares calculations on F^2.[14a] An empirical absorption correction was applied to the data using the program SADABS.[15] H atoms bonded to C atoms were geometrically placed after each cycle (C−H = 0.95 Å, U(iso) = 1.2 × U(eq) of C aromatic C−H's; C−H = 0.98 Å, U(iso) = 1.5 × U(eq) of C for CH_3). H atoms bonded to N and O atoms were located from difference Fourier maps, and their coordinates and U(iso) values were refined.

Crystal data collection and structure refinement for **1** and **2** were carried out in a similar manner. Abbreviated crystal data for **1**, **2**, and **7** are given in Table 1.

$[Fe_2(PZHPZ)_3](NO_3)_4 \cdot 5H_2O$ (5) and $[Co_2(PAHAP)_3](NO_3)_6] \cdot 9H_2O$ (6). The crystals of **6** are deep blood red.. The diffraction intensities of an approximately 0.40 × 0.20 × 0.40 mm crystal were collected with graphite-monochromatized Mo Kα X-radiation using a Rigaku AFC6S diffractometer at 299(1) K and the $\omega-2\theta$ scan technique to a $2\theta_{max}$ value of 50.1°. A total of 3549 reflections were measured, of which 1839 were considered unique (R_{int} = 0.024) and 1218 were considered significant with $I_{net} > 2.0\sigma(I_{net})$. The intensities of three representative reflections, which were measured after every 150 reflections, remained constant throughout the data collection, indicating crystal and electronic stability (no decay correction was applied). An empirical absorption correction, based on azimuthal scans of several reflections, was applied and resulted in transmission factors ranging from 0.93 to 1.00. The data were corrected for Lorentz and polarization effects. The cell parameters were obtained from the least-squares refinement of the setting angles of 24 carefully centered reflections with 2θ in the range 32.1−35.1°.

The structure was solved by direct methods.[16,17] All atoms except hydrogens were refined anisotropically. Hydrogen atoms were optimized by positional refinement, with isotropic thermal parameters set 20% greater than those of their bonded partners at the time of their inclusion. However they were fixed for the final round of refinement. The final cycle of full-matrix least-squares refinement was based on 1218 observed reflections ($I > 2.00\sigma(I)$) and 139 variable parameters and converged with unweighted and weighted agreement factors of $\sum||F_o| - |F_c||/\sum|F_o| = 0.050$ and $R_w = [\sum w(|F_o| - |F_c|)^2/\sum wF_o^2]^{1/2} = 0.054$. The maximum and minimum peaks on the final difference Fourier map correspond to 0.52 and −0.45 e Å^{-3} respectively. Neutral-atom scattering factors[18] and anomalous-dispersion terms[19,20] were taken from the usual sources. All calculations were performed with the TEXSAN[21] crystallographic software package using a VAX 3100 work station. Crystal data collection for **5** was carried out in a similar manner, except that a ψ-scan absorption correction was applied. The structure of **5** was solved by direct methods, and refined on F^2 using the SHELX-97 package running on DOS 6.22.[14b] Abbreviated crystal data for **5** and **6** are given in Table 1.

Table 1. Summary of Crystallographic Data for $[Mn_2(PAHAP)_3](ClO_4)_4 \cdot 5H_2O$ (**1**), $[Fe_2(PAHAP)_3](NO_3)_4 \cdot 3H_2O$ (**2**), $[Fe_2(PZHPZ)_3](NO_3)_4 \cdot 5H_2O$ (**5**), $[Co_2(PAHAP)_3](NO_3)_6] \cdot 5H_2O$ (**6**), and $[Ni_2(PAHAP)_3][Ni(H_2O)_6](NO_3)_6 \cdot 4.5H_2O$ (**7**)

	1	**2**	**5**
empirical formula	$C_{36}H_{46}Cl_4Mn_2N_{18}O_{21}$	$C_{39}H_{45}Fe_2N_{22}O_{15}$	$C_{60}H_{80}Fe_4N_{56}O_{34}$
fw	1318.59	1173.67	2353.2
space group	$C2/c$	$Pa\bar{3}$	$P2/n$
a (Å)	13.4086(2)	21.0024(1)	14.039(3)
b (Å)	32.0249(1)	21.0024(1)	11.335(6)
c (Å)	14.3132(2)	21.0024(1)	14.6517(15)
α (deg)	90	90	90
β (deg)	115.635(1)	90	96.852(11)
γ (deg)	90	90	90
V (Å^3)	5541.2(1)	9264.18(8)	2314.9(13)
ρ_{calcd} (g cm^{-3})	1.581	1.683	1.688
Z	4	8	1
μ (mm^{-1})	0.738	0.723	0.730
λ (Å)	0.710 73	0.710 73	0.710 69
T (K)	298(2)	298(2)	299(2)
R_1 (R)	0.0664	0.0615	0.0448 (R_1)
wR_2 (R_w)	0.1524	0.1640	0.1154 (wR_2)

	6	**7**
empirical formula	$C_{36}H_{54}N_{24}O_{27}Co_2$	$C_{8.33}H_{10.67}Cl_{0.67}N_{5.33}Ni_{0.67}O_{5.33}$
fw	686.42	337.67
space group	$R\bar{3}c(h)$ (No. 197)	$R\bar{3}c$
a (Å)	17.38(6)	17.373(3)
b (Å)	17.38(6)	17.373(3)
c (Å)	32.15(2)	33.235(6)
α (deg)	90	90
β (deg)	90	90
γ (deg)	90	120
V (Å^3)	8415(5)	8685(5)
ρ_{calcd} (g cm^{-3})	1.625	1.743
Z	12	27
μ (mm^{-1})	0.692	1.207
λ (Å)	0.710 69	0.710 73
T (K)	299(1)	150(2)
R_1 (R)	0.050 (R)	0.0488
wR_2 (R_w)	0.054 (R_w)	0.1133

[a] $R_1 = \sum|F_o| - |F_c|/\sum|F_o|$; w$R_2 = [\sum[w(|F_o|^2 - |F_c|^2)^2]/\sum[w(|F_o|^2)^2]]^{1/2}$. [b] $R = \sum||F_o| - |F_c||/\sum|F_o|$; $R_w = [\sum w(|F_o| - |F_c|)^2/\sum wF_o^2]^{1/2}$.

Results and Discussion

Structures. $[Mn_2(PAHAP)_3](ClO_4)_4 \cdot 5H_2O$ (1). The structure of **1** is illustrated in Figure 2, and important bond distances and angles are listed in Table 2. The dimanganese cation consists of two distorted octahedral manganese(II) centers bridged by three ligands in a spiral-like arrangement, with the

(12) *SMART: Data Collection Software*. Version 4.050; Siemens Analytical X-ray Instruments Inc.: Madison, WI, 1996.
(13) *SAINT: Data Reduction Software*, Version 4.050; Siemens Analytical X-ray Instruments Inc.: Madison, WI, 1996.
(14) (a) Sheldrick, G. M. *SHELXTL 5.04/VMS. An integrated system for solving, refining and displaying crystal structures from diffraction data*; Siemens Analytical X-ray Instruments Inc.: Madison, WI, 1995. (b) Sheldrick, G. M. *SHELX-97: A software package for the solution and refinement of X-ray data*; University of Göttingen: Göttingen, Germany, 1997.
(15) Sheldrick, G. M. *SADABS: Empirical Absorption Correction Program*; University of Göttingen: Göttingen, Germany, 1996.
(16) Gilmore, C. J. *J. Appl. Crystallogr.* **1984**, *17*, 42.
(17) Beurskens, P. T. *DIRDIF*; Technical Report 1984/1; Crystallography Laboratory: Toernooiveld, 6525 Ed Nijmegen, The Netherlands, 1984.
(18) Cromer, D. T.; Waber, J. T. *International Tables for X-ray Crystallography*; The Kynoch Press: Birmingham, United Kingdom, 1974; Vol. IV, Table 2.2A.
(19) Ibers, J. A.; Hamilton, W. C. *Acta Crystallogr.* **1964**, *17*, 781.
(20) Cromer, D. T. *International Tables for X-ray Crystallography*; The Kynoch Press: Birmingham, United Kingdom, 1974; Vol. IV, Table 2.3.1.
(21) *Texsan-Texray Structure Analysis Package*; Molecular Structure Corp.: The Woodlands, TX, 1985.

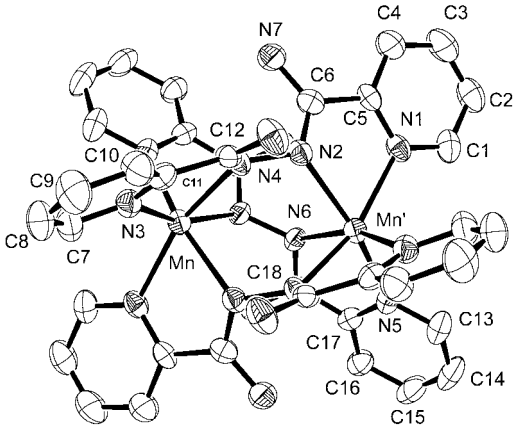

Figure 2. Structural representation of the dinuclear cation in $[Mn_2(PAHAP)_3](ClO_4)_4 \cdot 5H_2O$ (**1**) (40% probability thermal ellipsoids).

Table 2. Interatomic Distances (Å) and Angles (deg) Relevant to the Manganese Coordination Spheres in $[Mn_2(PAHAP)_3](ClO_4)_4 \cdot 5H_2O$ (**1**)

Mn−N(4)′	2.221(4)	Mn−N(5)	2.252(4)
Mn−N(6)	2.235(4)	Mn−N(2)	2.259(4)
Mn−N(3)′	2.240(4)	Mn−Mn′	3.946(4)
Mn−N(1)	2.244(4)	N(6)−N(6)′	1.437(8)
N(4)′−Mn−N(6)	90.3(2)	N(3)′−Mn−N(5)	102.5(2)
N(4)′−Mn−N(3)′	72.3(2)	N(1)−Mn-N(5)	106.5(2)
N(6)−Mn-N(3)′	161.3(2)	N(4)′−Mn−N(2)	86.9(2)
N(4)′−Mn−N(1)	158.2(2)	N(6)−Mn-N(2)	90.4(2)
N(6)−Mn-N(1)	96.9(2)	N(3)′−Mn−N(2)	95.2(2)
N(3)′−Mn−N(1)	101.8(2)	N(1)−Mn-N(2)	72.5(2)
N(4)′−Mn−N(5)	95.3(2)	N(5)−Mn-N(2)	162.0(2)
N(6)−Mn-N(5)	71.7(2)		
N(7)−H(7B)···O(91)	2.297	N(9)−H(9B)···O(6)	2.345
N(7)−H(7C)···O(7)	2.285	N(9)−H(9C)···O(6)	2.201
N(8)−H(8C)···O(91)	2.249		

diazine nitrogens acting as the bridging groups and the pyridine rings ligating to the remaining coordination positions. Mn−N distances are all very similar, falling in the range 2.22−2.26 Å. The Mn−Mn separation is 3.946(4) Å, and the least-squares planes of the two five-membered chelate rings of each ligand (e.g., Mn(a)−N(3)−C(11)−C(12)−N(9)) are twisted by 67.8°. On the outside of the complex ion, pairs of NH_2 groups are arranged in three sets, with a separation of 3.735 Å between adjacent pairs (e.g., N(7)−N(8)).

Within each ligand, the bond distances in the N═C−NH_2 framework are very similar to those of the free ligand[8] (e.g., N(2)−N(4) 1.425(6) Å, N(2)−C(6) 1.309(6) Å, C(6)−N(7) 1.331(7) Å, and C(5)−C(6) 1.492(7) Å), indicating single-bond character in the N−N diazine bonds and the C−NH_2 bonds and largely double-bond character in the C═N bonds. The large dihedral angle between the chelate rings within the same ligand is a clear reflection of the flexibility of the ligand about the N−N bond, an attribute which allows the spiral wrapping of the three ligands around the two metal centers and the geometric flexibility apparent in the copper complexes of this ligand.[8]

$[Fe_2(PAHAP)_3](NO_3)_4 \cdot 3H_2O$ (2). The structure of **2** is very similar to that of **1**, and a molecular projection with pyridine rings removed, viewed down the Fe−Fe axis, is illustrated in Figure 3. Important bond distances and angles are listed in Table 3. Metal−ligand bond distances are substantially shorter than those in **1**, with Fe−N distances falling in the range 1.95−2.0 Å, with a distance of 3.552(4) Å between the two iron centers. Angles around the iron centers are in the range 79.2−93°, indicating some distortion from an idealized octahedron.

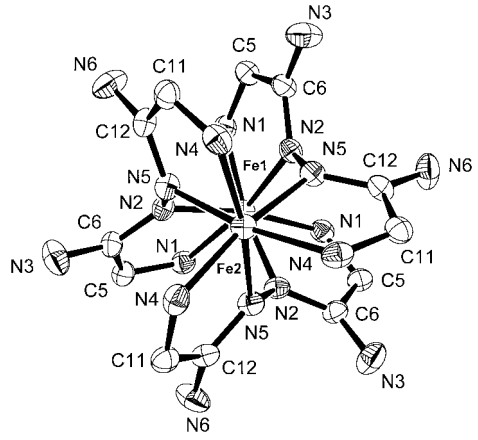

Figure 3. Structural representation of the dinuclear core in $[Fe_2(PAHAP)_3](NO_3)_4 \cdot 3H_2O$ (**2**) (40% probability thermal ellipsoids).

Table 3. Interatomic Distances (Å) and Angles (deg) Relevant to the Iron Coordination Spheres in $[Fe_2(PAHAP)_3](NO_3)_4 \cdot 3H_2O$ (**2**)

Fe(1)−N(2)	1.960(4)	Fe(2)−N(4)	1.996(4)
Fe(1)−N(1)	1.989(4)	Fe(1)−Fe(2)	3.552(4)
Fe(2)−N(5)	1.951(4)	N(2)−N(5)	1.409(6)
N(2)−Fe(1)−N(2)	89.9(2)	N(5)#1−Fe(2)−N(5)#2	90.5(2)
N(2)−Fe(1)−N(1)	79.2(2)	N(5)#1−Fe(2)−N(4)	169.9(2)
N(2)#1−Fe(1)−N(1)	93.5(2)	N(5)#2−Fe(2)−N(4)	93.2(2)
N(2)#2−Fe(1)−N(1)	168.6(2)	N(5)−Fe(2)−N(4)	80.1(2)
N(1)−Fe(1)−N(1)#1	97.8(2)	N(4)−Fe(2)−N(4)#2	96.7(2)

The ligands exhibit a marked spiral twist around the dinuclear iron center, with a dihedral angle of 67.5° between the five-membered iron chelate rings belonging to the same ligand. Despite the shorter metal−nitrogen distances in **2** compared with **1**, the ligand twist is very similar. Within each ligand, the bond distances in the NH_2−C═N framework (e.g., N(2)−N(5) 1.409(6) Å, N(2)−C(6) 1.309(7) Å, and C(6)−N(3) 1.323(7) Å) are very similar to those in **1** and in the free ligand, although in this case the C−N distances are much closer, suggesting some double-bond delocalization into the C−NH_2 bond.

$[Fe_2(PZHPZ)_3](NO_3)_4 \cdot 5H_2O$ (5). The structure of the molecular cation in **5** is illustrated in Figure 4. Important bond distances and angles are listed in Table 4. The structure is essentially identical with those of **1** and **2** with a distance of 3.570(3) Å between the iron(II) centers. The Fe−N distances lie in the range 1.94−1.97 Å, very similar to those in **2**. There is no evidence for further interactions between the dinuclear units that would involve any additional coordination of the external pyrazine nitrogens. The N−N distances (1.412(4), 1.418(5) Å) indicate single N−N bonds within each ligand, and the distances within the N═C−NH_2 ligand framework are very close to those in the free ligand. The spiral twist of the ligand around the two iron centers is very similar to that found in **1** and **2**, with e.g. a 66.3° angle between the least-squares planes Fe(1)−N(2)−C(6)−C(5)−N(1) and Fe(1)a−N(11)−N(12)−C(15)−C(16).

$[Co_2(PAHAP)_3](NO_3)_6 \cdot 9H_2O$ (6). The structure of the cation in **6** is illustrated in Figure 5. Important bond distances and angles are listed in Table 5. Bond distances to the nitrogen donor atoms are very short (Co(1)−N(1) 1.915(4) Å, Co(1)−N(3) 1.942(4) Å), in keeping with the 3+ oxidation state of the cobalt centers. The cobalt octahedra are somewhat distorted, with N−Co−N angles ranging from 82 to 95.9°. The Co−Co separation is 3.508(3) Å. Within the N−C−N−N framework of the ligand, the N−N distance is quite short (1.397(7) Å), in keeping with very short Co−N contacts. The N−C (e.g., N(1)−C(1)) distance is somewhat longer and the C−NH_2 distance

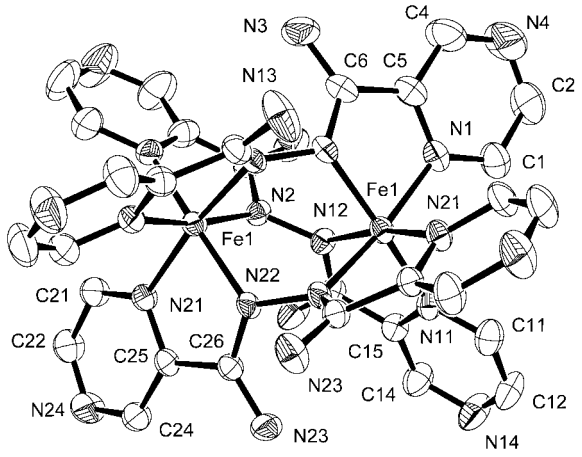

Figure 4. Structural representation of the dinuclear cation in $[Fe_2(PZHPZ)_3](NO_3)_4 \cdot 5H_2O$ (**5**) (40% probability thermal ellipsoids).

Table 4. Interatomic Distances (Å) and Angles (deg) Relevant to the Iron Coordination Spheres in $[Fe_2(PZHPZ)_3](NO_3)_4 \cdot 5H_2O$ (**5**)

Fe(1)−N(2)	1.943(3)	Fe(1)−N(22)	1.963(3)
Fe(1)−N(1)	1.951(3)	Fe(1)−Fe(1′)	3.570(3)
Fe(1)−N(12)	1.951(3)	N(2)−N(12)#1	1.412(4)
Fe(1)−N(21)	1.954(3)	N(22)−N(22)#1	1.418(5)
Fe(1)−N(11)	1.959(3)		
N(2)−Fe(1)−N(1)	79.97(12)	N(12)−Fe(1)−N(11)	80.16(11)
N(2)−Fe(1)−N(12)	89.68(11)	N(21)−Fe(1)−N(11)	96.37(12)
N(1)−Fe(1)−N(12)	95.75(11)	N(2)−Fe(1)−N(22)	90.54(11)
N(2)−Fe(1)−N(21)	94.29(12)	N(1)−Fe(1)−N(22)	169.01(11)
N(1)−Fe(1)−N(21)	94.99(11)	N(12)−Fe(1)−N(22)	89.68(11)
N(12)−Fe(1)−N(21)	169.05(11)	N(21)−Fe(1)−N(22)	80.10(11)
N(2)−Fe(1)−N(11)	169.19(11)	N(11)−Fe(1)−N(22)	93.06(11)
N(1)−Fe(1)−N(11)	97.27(12)		

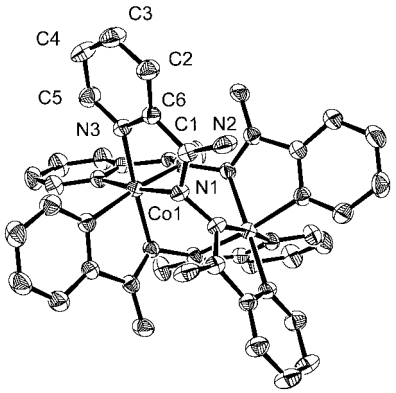

Figure 5. Structural representation of the dinuclear cation in $[Co_2(PAHAP)_3](NO_3)_6 \cdot 5H_2O$ (**6**) (40% probability thermal ellipsoids).

Table 5. Interatomic Distances (Å) and Angles (deg) Relevant to the Cobalt Coordination Spheres in $[Co_2(PAHAP)_3](NO_3)_6] \cdot 5H_2O$ (**6**)

Co(1)−N(1)	1.915(4)	N(1)−N(1)	1.397(7)
Co(1)−N(3)	1.942(4)	Co(1)−Co(1)′	3.508(3)
N(1)−Co(1)−N(1)	90.1(1)	N(1)−Co(1)−N(3)	82.0(2)
N(1)−Co(1)−N(3)	171.8(2	N(3)−Co(1)−N(3)	95.9(1)
N(1)−Co(1)−N(3)	92.2(2)		

(C(1)−N(2) 1.305(5) Å) somewhat shorter than in **1**, **2**, and **5**, resulting in more double-bond character in the C−NH_2 bond. A comparison with the $[Co_2(PMK)_3]^{4+}$ structure reveals much longer Co−N distances (2.07−2.18 Å) and a very much longer Co−Co separation (3.81(1) Å.[5] The torsional angle Co−N−N−Co for this compound is small (44)°, but perhaps a direct comparison with **6** is unwise because of the differences in the ligands. For **6**, the dihedral angles between the mean planes of the cobalt chelate rings associated with the same ligand (50.8°) are in keeping with the general spiral geometry of the dimetal cation but are substantially smaller than those in the other complexes and may be associated with the short metal−nitrogen contacts and average N−Co−N angles closer to 90°.

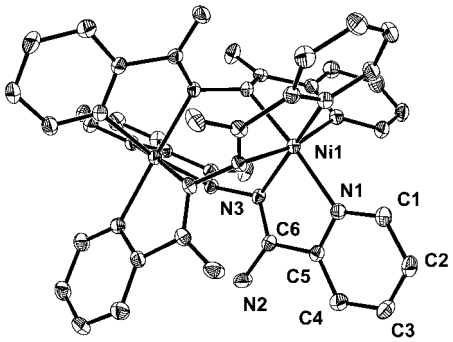

Figure 6. Structural representation of the dinuclear cation in $[Ni_2(PAHAP)_3][Ni(H_2O)_6](NO_3)_6 \cdot 4.5H_2O$ (**7**) (40% probability thermal ellipsoids).

Table 6. Interatomic Distances (Å) and Angles (deg) Relevant to the Nickel Coordination Spheres in $[Ni_2(PAHAP)_3][Ni(H_2O)_6](No_3)_6 \cdot 4.5H_2O$ (**7**)

Ni(1)−N(1)	2.063(3)	N(3)−N(3)′	1.418(5)
Ni(1)−N(3)	2.078(3)	Ni(1)−Ni(1)′	3.691(5)
Ni(2)−O(1)	2.056(3)		
N(1)′−Ni(1)−N(1)	97.04(10)	N(1)′−Ni(1)−N(3)	168.76(10)
N(1)′−Ni(1)−N(3)	93.85(10)	N(3)−Ni(1)−N(3)′	90.98(10)
N(1)−Ni(1)−N(3)	78.81(10)		

$[Ni_2(PAHAP)_3][Ni(H_2O)_6](NO_3)_6 \cdot 4.5H_2O$ (7). **7** consists of two metal fragments, a dinuclear cation, with a similar spiral twist to the other complexes, and the mononuclear cation $[Ni(H_2O)_6]^{2+}$. A structural representation for the dinuclear cation is illustrated in Figure 6. Important bond distances and angles are listed in Table 6. Nickel−nitrogen bond distances fall in the range 2.06−2.08 Å, and the N−Ni−N angles fall in the range 78.8−97.1°, indicating significant distortion of the nickel octahedra. The mononuclear cation $[Ni(H_2O)_6]^{2+}$ has an almost regular octahedral geometry (Ni−O 2.056(3) Å, O−Ni−O 89.24−90.75°). The Ni−Ni distance is 3.691(5) Å. The N−N distance (N(3)−N(3′) is 1.428(5) Å, and the C−N distances in the ligand framework (N(3)−C(6) 1.307(4) Å, C(6)−N(2) 1.325(4) Å) are very close to those in the free ligand, indicating single N−N bond character in the ligand bridge. The dihedral angles between the mean planes of the nickel chelate rings (70.06(8)°) are close to those reported for the other complexes, in keeping with the relatively long Ni−N bonds and large range of angles at the nickel centers.

$[Fe(PHAAP\text{-}H)(H_2O)_2(NO_3)](NO_3)_2$ (9). The full details of the structure of **9** will be published elsewhere.[11] The seven-coordinate Fe(III) center is bonded equatorially to pyridine and diazine nitrogen sites and a deprotonated oxygen site of the ligand, and to a bidentate nitrate, with two axially bound water molecules. A preliminary structural representation is illustrated in Figure 7. The pendant pyridine nitrogen is protonated and fixed, along with the NH_2 group, in a planar external structural arrangement by hydrogen-bonding contacts to an ionic nitrate (not shown).

Synthesis, Spectroscopy, Electrochemistry, and Magnetism. PAHAP closely resembles PAA and PMK in terms of its coordinating ability, and the spiral dinuclear complexes of PAHAP are very similar in structure to the previously reported examples which contain the cation $[Co_2(PMK)_3]^{2+}$ [5] and to the

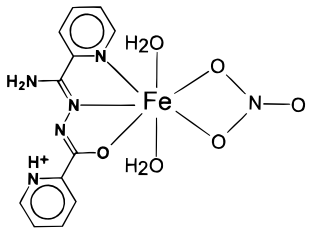

Figure 7. Structural representation of the cation in $[Fe(PHAAP-H)(H_2O)_2(NO_3)](NO_3)_2$ (**9**).

complex $[Fe_2(salhn)_3]$.[7] It is reasonable to assume that other reported complexes of PMK and PAA with the same complex stoichiometry have similar spiral structures. Previous reports on iron and cobalt complexes of PAA and PMK involve reactions of Fe(II) only, and in the case of Co(II), air was excluded in the syntheses, preventing any oxidation to Co(III).[1,2,5] In the present study, all reactions were done in air, and in the case of iron, both Fe(II) and Fe(III) salts were used in the syntheses.

Reactions of iron(III) nitrate with both PAHAP and PZHPZ in aqueous solution led to spontaneous reductions over several days with the formation of low yields of $[Fe_2(L)_3]^{4+}$ (L = PAHAP, PZHPZ). This suggests that a reducing medium is formed through hydrolysis of the ligand. The discovery of the mononuclear Fe(III) complex **9**, which contains the ligand PHAAP, as a byproduct in the reaction of Fe(III) nitrate with PAHAP indicates that, in addition, a small proportion of the ligand itself undergoes a different hydrolytic process. Fe(II) complexes of PAA, e.g. $[Fe_2(PAA)_3]^{4+}$, are unstable in aqueous solution and have been shown to decompose rapidly with the formation of the species $[Fe(PAH)_3]^{2+}$ (PAH = 2-pyridinal hydrazone) and 2-pyridinecarboxaldehyde.[1] In fact, the complex cation $[Fe_2(PAA)_3]^{4+}$ could only be stabilized as a solid by rapid addition of excess iodide to the aqueous solution.[1] Further evidence for the solution decomposition of $[Fe_2(PAA)_3]^{4+}$ was obtained from magnetic measurements, which showed that the low-spin dinuclear complex was transformed into a high-spin mononuclear Fe(II) solution species.[2]

The spontaneous reduction of Fe(III)/PAHAP and Fe(III)/PZHPZ solutions can be understood in terms of a simple hydrolysis of the coordinated ligand to produce picolinamide hydrazone (starting material for PAHAP) and picolinamide, or picolinamide and hydrazine (similarly for the corresponding pyrazine derivatives of PZHPZ). The picolinamide hydrazone would have significant reducing ability, in addition to hydrazine itself. Preliminary coordination of Fe(III) to a diazine nitrogen would enhance such attack by water by making the adjacent carbon more electrophilic. The low yields of **2** and **5** suggest that some ligand is sacrificed to reduce Fe(III) to Fe(II) and produce the dinuclear Fe(II) complex of the remaining PAHAP and PZHPZ.

The formation of the mononuclear Fe(III) complex **9** in the same reaction can be explained by preliminary coordination of PAHAP as a tridentate chelating ligand via a pyridine, a diazine, and an NH_2 site or as a bidentate ligand via one pyridine and one diazine nitrogen, followed by hydrolysis at the diazine carbon to produce the alkoxide oxygen and releasing ammonia. This oxygen then coordinates to the Fe(III) center. This reaction could also be facilitated by the acidity of the aqueous solution of $Fe(NO_3)_3$, which also causes protonation of a pyridine nitrogen in **9**, thus effectively preventing the coordination of two metals. PHAAP has been prepared independently, and **9** has been prepared in high yield by the direct reaction of PHAAP and $Fe(NO_3)_3$ in aqueous solution.[11] It is significant that the dinuclear Fe(III) complex **4** can be produced as a relatively stable solid. This is attributed to its much lower solubility in aqueous solution, and so it precipitates before any significant reduction can occur. The formation of the Co(III) complex **6** under similar conditions, in rather low yield, indicates the instability of Co(II) PAHAP systems to oxidation (cobalt(II) derivatives of PAA and PMK were prepared under nitrogen atmosphere[2,5]), but thus far there is no evidence for ligand hydrolysis. It seems reasonable to assume in this case that the oxidation step, common in cobalt(II) chemistry, occurs through the prior formation of a 1:2 or 2:2 (ligand:metal) intermediate complex, leaving vacant coordination sites for interaction with O_2, with the subsequent formation of the stable spiral complex.

The infrared spectra of all the compounds show high-energy absorptions (>3200 cm^{-1}) associated with lattice and coordinated waters and the NH_2 groups. ν_3 perchlorate absorptions associated with ClO_4^- are found at 1078 cm^{-1} (**1**), 1164 cm^{-1} (**3**), and 1089 cm^{-1} (**4**), and $\nu_1 + \nu_4$ nitrate combination bands[24] associated with free nitrate are found at 1753 cm^{-1} (**2**), 1765 cm^{-1} (**5**), and 1764 cm^{-1} (**7**), while for **9** three prominent bands are found at 1794, 1774, and 1703 cm^{-1} associated with bidentate and ionic nitrate.

Solid-state electronic and solution spectral bands are listed in Table 7. The iron(II) complexes are dominated by intense low-energy charge-transfer absorptions in the range 560−650 nm. The iron(III) complex (**4**) has a longer wavelength absorption than **2** and **3** (645, 540 nm (sh)). In aqueous solution, **2** and **3** have identical spectra, and comparable spectra are obtained in DMF. The general similarity in solid state and solution spectra for **2** and **3** suggests that the spiral dinuclear cation retains its integrity in solution. The aqueous solution spectra remain essentially unchanged over an extended period of time (days), suggesting that the hydrolytic instability which characterizes the comparable PAA systems[22] does not occur significantly with the Fe(II) PAHAP complexes. The longer wavelength charge-transfer absorption for **5** in the solid state indicates the effect of replacing pendant pyridines with pyrazines, consistent with metal to ligand charge transfer as the origin of this absorption. In aqueous solution similar shifts to higher energy are observed (581, 411 nm).

4 dissolves in water to give a brown solution, which gradually becomes purple on standing over a period of several days. Initial broad bands at ≈550 and 360 nm in aqueous solution change in relative intensity, with the 550 nm band increasing and the 360 band decreasing to be replaced exactly by the characteristic bands associated with the iron(II) complex **3**. The suggested mechanism for reduction involves ligand hydrolysis presumably to form mononuclear Fe(II) intermediates, but the intense charge transfer bands of both the Fe(III) and Fe(II) dinuclear complexes preclude the observation of such species which are likely to be weaker absorbers in this spectral region. **6** shows a broad shoulder absorption in the solid state at ≈550 nm, associated with a spin-allowed transition in low-spin Co(III) ($^1A_{1g} \rightarrow {}^1T_{1g}$), which appears essentially unchanged in aqueous solution. **7** shows two solid-state d−d absorption envelopes at 814, 890 (sh) nm, and 550 (sh) nm. Using an octahedral model these absorptions can be associated with the ν_1 ($^3A_{2g} \rightarrow {}^3T_{2g}$) and ν_2 ($^3A_{2g} \rightarrow {}^3T_{1g}$) transitions, respectively. The splitting of ν_1 may be associated with a lowering of the octahedral symmetry or

(22) Stratton, W. J.; Rettig, M. F.; Drury, R. F. *Inorg. Chim. Acta* **1969**, *3*, 97.
(23) Stratton, W. J.; Busch, D. H. *J. Am. Chem. Soc.* **1958**, *80*, 3191.
(24) Lever, A. B. P.; Mantovani, E.; Ramaswamy, B. S. *Can. J. Chem.* **1971**, *49*, 1957.

Table 7. UV/Vis Spectral Data[a]

compound	mull transmittance λ_{max} (nm)	solution λ_{max} (nm) (ϵ (L·mol^{-1}·cm^{-1}))
$[Fe_2(PAHAP)_3](NO_3)_4 \cdot 3H_2O$ (**2**)	570	532 (5200), [550], 380 (3600)[b]
$[Fe_2(PAHAP)_3](ClO_4)_4 \cdot 4H_2O$ (**3**)	565	532 (5200), [550], 380 (3600)[b]
$[Fe_2(PAHAP)_3](ClO_4)_6 \cdot 4.5H_2O$ (**4**)	645, [540]	550, 360[b]
$[Fe_2(PZHPZ)_3](NO_3)_4 \cdot 5H_2O$ (**5**)	641	581, 411[b]
$[Co_2(PAHAP)_3](NO_3)_6 \cdot 5H_2O$ (**6**)	~550 br	~550 br[b]
$[Ni_2(PAHAP)_3][Ni(H_2O)_6](NO_3)_6 \cdot 4.5H_2O$ (**7**)	[890], 814, [550]	900 (75), 815 (106), 545 (69), 305 (2.4×10^4)[b]
$[Ni_2(PAHAP)_3](ClO_4)_4 \cdot 5H_2O$ (**8**)	[890], 820, 546	[890], 823 (223), 545 (172)[b]
$[Fe(PHAAP\text{-}H)(H_2O)_2(NO_3)](NO_3)_2$ (**9**)	630	634 (900)[b]

[a] Values in brackets are shoulders. [b] Aqueous solution.

with a spin-forbidden transition. These band positions compare closely with those for $[Ni(dipy)_3]^{2+}$.[25] The aqueous solution spectrum is very similar, with quite high extinction coefficients, indicating that the weakly absorbing $[Ni(H_2O)_6]^{2+}$ cation would not appear in the spectrum. A strong charge-transfer band is also found at 305 nm ($\epsilon = 2.4 \times 10^4$ L·mol^{-1}·cm^{-1}). **8** has an essentially identical spectrum, both in the solid state and in solution, except that the aqueous solution absorption intensities are higher, as would be expected. **9** has a strong absorption at 630 nm in the solid state, and a dark green aqueous solution of the complex has an intense single band at 634 nm, which is clearly charge transfer in nature. This complex shows no tendency to reduce, unlike its parental counterpart.

The fact that **4** is reduced slowly in aqueous solution to a more stable dinuclear Fe(II) species, with no tendency for spontaneous reoxidation, prompted us to examine the redox properties of complex **3**. Cyclic voltammetry for an aqueous solution of **3** (Pt reference electrode, glassy carbon working electrode, SCE reference electrode, 0.1 M $NaNO_3$, 10^{-3} M complex) reveals two well-separated waves [$E_{1/2}(1) = 0.16$ V ($\Delta E_p = 70$ mV (25 mV s^{-1})); $E_{1/2}(2) = 0.38$ V ($\Delta E_p = 70$ mV (25 mV s^{-1}))], which show very little change as a function of scan rate. The redox processes are associated with two one-electron oxidation steps with the formation of Fe(II)−Fe(III) and Fe(III)−Fe(III) species, by what are essentially reversible processes. This clearly indicates the stability of the spiral dinuclear cation in solution in water in two oxidation states, during the lifetime of the experiment. Current heights for the anodic and cathodic components of these waves are equal.

The low-spin Co(III) complex **6** was examined electrochemically under the same conditions as **3** and exhibits two sets of waves around 0.0 V, associated with Co(II) and Co(III) species. A quasi-reversible wave (some variation of ΔE_p with scan rate) at $E_{1/2} = 0.10$ V ($\Delta E_p = 100$ mV at 25 mV s^{-1}) is associated with the formation of a Co(II)−Co(III) species, while a similar wave at $E_{1/2} = -0.050$ V ($\Delta E_p = 100$ mV) corresponds to the formation of the fully reduced Co(II)−Co(II) species. Current heights for the anodic and cathodic components of these waves are equal. It is reasonable to assume that the integrity of the dinuclear cation is maintained during the redox process. Electrochemical investigations of the dimanganese(II) and dinickel(II) species were unsuccessful, and at the high potentials necessary to see electrochemical activity, ligand oxidation appeared to be occurring.

Room-temperature magnetic moments (reported per metal center) were determined for all compounds. **1** has a high value ($\mu_{eff} = 6.1\ \mu_B$) consistent with the presence of high-spin manganese(II) centers. The iron(II) complexes are all low spin ($\mu_{eff} = 0.7\ \mu_B$ (**2**), $0.9\ \mu_B$ (**3**), $0.69\ \mu_B$ (**5**), while the iron(III) complex **4** has a high value ($\mu_{eff} = 4.70\ \mu_B$), indicative of a high-spin system. This value is smaller than the spin-only value for five unpaired electrons and may indicate the presence of antiferromagnetic coupling or a spin transition phenomenon. However, what is more likely is that since the Fe(III)/PAHAP systems is inherently unstable (vide infra), the complex is somewhat unstable, even in the solid state, and contains a small amount of a low-spin Fe(II) complex, either as an Fe(II)−Fe(II) species or possibly an Fe(II)−Fe(III) species. The low value for **6** ($\mu_{eff} = 0.6\ \mu_B$) is consistent with low-spin cobalt(III). The nickel(II) complexes have magnetic moments close to expected values for uncoupled Ni(II) centers ($\mu_{eff} = 3.1\ \mu_B$ (**7**), $3.1\ \mu_B$ (**8**)).

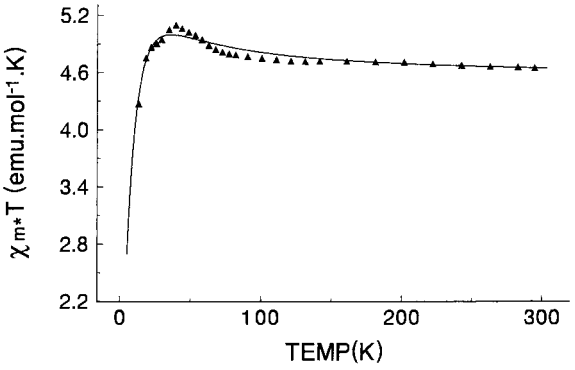

Figure 8. Variable-temperature magnetic susceptibility data for $[Mn_2(PAHAP)_3](ClO_4)_4 \cdot 5H_2O$ (**1**). The best-fit solid line was obtained from eq 1, with $g = 2.029(6)$, $2J = 2.08(8)$ cm^{-1}, $N\alpha = 18 \times 10^{-6}$ emu, $\rho = 0.0116$, $\Theta = -9.6$ K, $10^2R = 0.95$ ($R = [\Sigma(\chi_{obs} - \chi_{calc})^2/\Sigma\chi_{obs}]^{1/2}$).

Variable-temperature magnetic studies were carried out on powdered samples of **1** (13−300 K) and **8** (4−300 K). The χ_m*T profile for **1** shows an unusual temperature dependence (Figure 8) with χ_m*T rising from 4.66 emu·mol^{-1}·K at 296 K to a maximum at 40 K of 5.1 emu·mol^{-1}·K and then falling rapidly to 4.25 emu·mol^{-1}·K at 13 K. This behavior is consistent with a ferromagnetically coupled system, but the drop in χ_m*T at low temperature suggests the presence of an antiferromagnetic component in the total spin exchange or possibly Zeeman level depopulation effects. The data were fitted only to a simple isotropic exchange expression for two $S = {}^5/_2$ spin states derived from the exchange Hamiltonian $H = -2JS_1 \cdot S_2$ (eq 1; $A = x^{28} + 5x^{18} + 14x^{18} + 30x^{10} + 55$; $B = x^{30} + 3x^{28} + 5x^{24} + 7x^{18} + 9x^{10} + 11$; $x = -2J/kT$), where χ_m is the magnetic susceptibility per metal center and other terms have their usual meaning (ρ = fraction of mononuclear impurity). A reasonable data fit (Figure 8) was obtained for $g = 2.029(6)$, $2J = 2.08(8)$ cm^{-1}, $N\alpha = 18 \times 10^{-6}$ emu, $\rho = 0.0116$, $\Theta = -9.6$ K, $10^2R = 0.95$ ($R = [\Sigma(\chi_{obs} - \chi_{calc})^2/\Sigma\chi_{obs}]^{1/2}$). Variable-temperature magnetic data for **8** indicate no significant magnetic interaction between the nickel(II) centers. The χ_m*T values are temperature invariant (1.2 emu·mol^{-1}·K) from 296 to 10 K,

$$\chi_m = \left[\frac{Ng^2\beta^2}{k(T-\Theta)}\frac{A}{B}\right](1-\rho) + \frac{1.094\rho g^2}{T} + N\alpha \qquad (1)$$

(25) Lever, A. B. P.; Lewis, J.; Nyholm, R. S. *J. Chem. Soc.* **1964**, 1187.

with a very slight increase at lower temperature, suggesting a possible weak intermolecular interaction. No fitting of these data was attempted.

From a structural perspective, any intramolecular spin interaction between the metal centers would be dependent on magnetic orbital overlap via the bridging N_2 diazine linkage. This is clearly inconsequential for the low-spin systems, but for **1** and **8**, interactions via t_{2g} and e_g orbitals are magnetically active (assuming an octahedral model). In previous studies[8,9] on dicopper(II) complexes of PAHAP and related ligands, the twist angle around the bridging N−N group was found to be a critical factor in exchange propagation between copper(II) centers, and effective orthogonality between the copper magnetic orbitals was achieved at twist angles around 70°, which was directly related to orthogonality between the nitrogen p orbitals involved. The average twist angle between the manganese chelate rings ($Mn-N_{diazine}-C-C-N_{pyr}$) was found to be 67.8°, very close to the orthogonal limit found in the dicopper(II) case and clearly reasonable in terms of the dominant weak ferromagnetism observed for **1**. The significant negative Θ value indicates a weak intermolecular antiferromagnetic interaction. The only way that such an interaction could take place is via the NH_2 groups of the ligand, which are poised appropriately with respect to the Mn orbitals via a flat ligand portion ($N=C-NH_2$). Significant hydrogen-bonding contacts are found linking N(7) and N(8) in neighboring molecules to water molecule O(91) and linking N(7) and N(9) to perchlorate oxygens O(6) and O(7) (Table 2). The connection N(7)−O(7)−Cl(2)−O(6)−N(9) provides a rather long but potentially viable route for such an interaction.

Although no structural data are available for **8**, it is reasonable to assume that the dinuclear center dimensions are similar to those of the same cation in **7**. In this complex the dihedral angles between the $Ni-N_{diazine}-C-C-N_{pyr}$ mean planes are 70.1°, clearly indicating an exchange situation close to the point of orthogonality for the nitrogen p orbitals in the N−N bridge. The apparent lack of coupling in **8** is entirely consistent with this structural extrapolation.

Conclusion

Although one structural report on the elusive spiral dinuclear complexes of this class of tetradentate N_4 diazine ligand (e.g., PMK) appeared in 1974, the structural details have remained somewhat of a mystery since the original discovery by Busch in 1958. Five complexes in this class are presented in this report, all showing the same spiral structure, with three canted ligands wrapped around the dinuclear metallic core and three diazine N_2 groups acting as bridges among the manganese, iron, cobalt, and nickel centers. The Fe(II) and Co(III) complexes are low-spin, while the Mn(II) and Ni(II) complexes are high spin. The magnetic properties of the Mn(II) derivative imply the presence of weak ferromagnetic coupling, while the Ni(II) complexes are uncoupled, consistent with the twist angles around the N−N bridges.

Acknowledgment. We thank the Natural Sciences and Engineering Research Council of Canada for financial support for this study and Dr. Glenn P. A. Yap at the University of Windsor for structural data on complexes **1** and **2**.

Supporting Information Available: X-ray crystallographic files in CIF format for the structure determinations of $[Mn_2(PAHAP)_3](ClO_4)_4 \cdot 5H_2O$ (**1**), $[Fe_2(PAHAP)_3](NO_3)_4 \cdot 3H_2O$ (**2**), $[Fe_2(PZHPZ)_3](NO_3)_4 \cdot 5H_2O$ (**5**), $[Co_2(PAHAP)_3](NO_3)_6 \cdot 5H_2O$ (**6**), and $[Ni_2(PAHAP)_3][Ni(H_2O)_6](NO_3)_6 \cdot 4.5H_2O$ (**7**) are available on the Internet only. Access information is given on any current masthead page.

IC9715761